DOI: 10.1002/chem.200903348

Scission of Carbon Monoxide Using TaR_3, R = (N(*t*Bu)Ph) or OSi(*t*Bu)$_3$: A DFT Investigation

Nigel J. Brookes,[a] Alireza Ariafard,[a, c] Robert Stranger,[b] and Brian F. Yates*[a]

Abstract: The experimentally known reduction of carbon monoxide using a 3-coordinate [Ta(silox)$_3$] (silox = OSi(*t*Bu)$_3$) complex initially forms a ketenylidene [(silox)$_3$Ta−CCO], followed by a dicarbide [(silox)$_3$Ta−CC−Ta(silox)$_3$] structure. The mechanism for this intricate reaction has finally been revealed by using density functional theory, and importantly a likely structure for the previously unknown intermediate [(silox)$_3$Ta−CO]$_2$ has been identified. The analysis of the reaction pathway and the numerous intermediates has also uncovered an interesting pattern that results in CO cleavage, that being scission from a structure of the general form [(silox)$_3$Ta−C$_n$O] in which *n* is even. When *n* is odd, cleavage cannot occur. The mechanism has been extended to consider the effect of altering both the metal species and the ligand environment. Specifically, we predict that introducing electron-rich metals to the right of Ta in the periodic table to create mixed-metal dinuclear intermediates shows great promise, as does the ligand environment of the Cummins-style 3-coordinate amide structure. This latter environment has the added complexity of improved electron donation from amide rotation that can significantly increase the reaction exothermicity.

Keywords: carbon monoxide · computational chemistry · density functional calculations · reaction mechanisms · transition metals

Introduction

The breakdown of small multiply bonded molecules, such as N_2, CO, CO_2 and N_2O, has attracted considerable interest from chemical research groups over the past 15 years. Some success has been achieved in the dinitrogen area with the significant work by Laplaza and Cummins[1] using a 3-coordinate molybdenum amide to cleave dinitrogen, and Schrock[2] using a molybdenum triamidoamine complex in the catalytic reduction of N_2 at ambient pressure and temperature. The concept applied in both of these areas has been to create a very active metal centre with coordinated basic ligands that provide sufficient steric bulk such that access can only be gained by the small dinitrogen molecule.

It is no surprise then to find this approach used in the breakdown of other small molecules and much of the emphasis in this approach has been from a theoretical perspective.[3–23] Of particular interest to carbon monoxide cleavage was work by Christian et al.,[11] in which a potential path for CO cleavage was devised by using a mixed metal tri-amide system of rhenium and tantalum. During this investigation, the potential for using a single d^2 metal amide, such as [Ta{N(*t*Bu)Ar}$_3$], was discarded due to the thermodynamic sink created when two of the metals bind end-on with CO, which leads to a stable dinuclear [RR′M−CO−MRR′] structure.

These results are of particular interest when compared with the earlier experimental work of LaPointe and Neithamer[24,25] who used the isoelectric 3-coordinate [Ta(silox)$_3$] (**1**$_S$,[26] silox = OSi(*t*Bu)$_3$) complex. This complex has the desired active centre, basic ligands and significant steric bulk so we would expect it to react in a similar fashion to the Cummins system. However, the interaction of [Ta(silox)$_3$] (**1**$_S$) with CO does not form a CO bound dinuclear species as predicted theoretically, but instead forms a dinu-

[a] Dr. N. J. Brookes, Dr. A. Ariafard, Prof. B. F. Yates
School of Chemistry, University of Tasmania
Private Bag 75, Hobart, Tasmania 7001 (Australia)
Fax: (+61) 3-6226-2858
E-mail: Brian.Yates@utas.edu.au

[b] Prof. R. Stranger
Research School of Chemistry
The Australian National University
Canberra ACT 0200 (Australia)

[c] Dr. A. Ariafard
Department of Chemistry, Faculty of Science
Central Tehran Branch, Islamic Azad University
Shahrak Gharb, Tehran (Iran)

Supporting information for this article is available on the WWW under http://dx.doi.org/10.1002/chem.200903348.

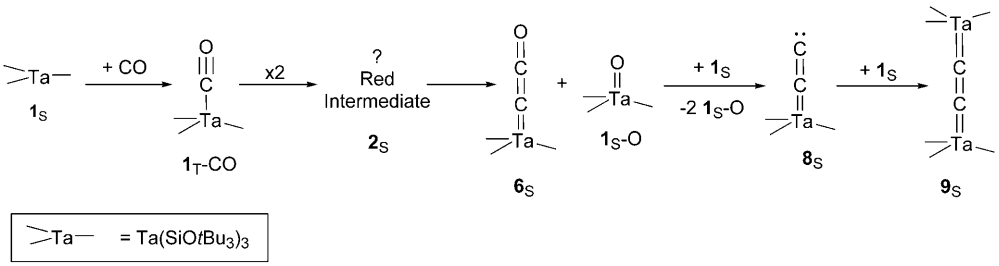

Scheme 1. Suggested mechanism for dicarbide formation.

clear, dicarbide structure [(silox)$_3$Ta–CC–Ta(silox)$_3$] (**9**$_S$), along with the oxo monomer [(silox)$_3$Ta=O] (**1**$_S$-O). The suggested mechanism for the dicarbide formation is outlined in Scheme 1. It firstly involves coordination of CO to form [(silox)$_3$Ta–CO] (**1**$_T$-CO) followed by formation of an unidentified red solid intermediate with the formula [(silox)$_3$TaCO]$_2$, prior to stable ketenylidene [(silox)$_3$Ta–CCO] (**6**$_S$) and [(silox)$_3$Ta–O] (**1**$_S$-O) products. The ketenylidene (**6**$_S$) can interact further with additional **1**$_S$, by removing the apical oxygen to create **1**$_S$-O plus an unstable vinylidene [(silox)$_3$Ta–CC:] (**8**$_S$), which in turn combines with another reactant to yield the final dinuclear dicarbide **9**$_S$.

Armed with this information, surely we would expect a Cummins 3-coordinate tantalum amide system to react in a similar fashion to the LaPointe tantalum silox system. In fact, one might expect the amide system to be more reactive than the silox equivalent, based on the additional electron donation provided by (the well-studied)[4,8,10,17] amide rotation. It is interesting to note that the reverse comparison has recently been synthetically achieved whereby the LaPointe silox system has been tuned to a d^3-molybdenum centre to create the complex [Mo(silox)$_3$].[27] As one might expect, the reactivity of [Mo(silox)$_3$] is similar to the analogous Cummins molybdenum [Mo{N(*t*Bu)Ar}$_3$] moiety, although it is not sufficiently active to cleave N_2. This would add further weight to a d^2-tantalum Cummins system being capable of cleaving CO.

These apparently conflicting findings warrant further investigation. Is the same reaction pathway possible for both [Ta(silox)$_3$] and [Ta{N(*t*Bu)Ar}$_3$] and could the metal triamide structure of Laplaza–Cummins be used or tuned for CO cleavage within this reaction pathway? Exactly what is the structure of the red intermediate known to exist in the LaPointe reaction and how does it form? Why is it possible to cleave the CO in [(silox)$_3$Ta–CCO] (**6**$_S$) but not possible in [(silox)$_3$Ta–CO]? This article answers these questions by considering a detailed theoretical study of the original [Ta(silox)$_3$]+CO reaction and applying it to a proposed Cummins-style [Ta{N(*t*Bu)Ar}$_3$] system.

Methods

To adequately analyse the reaction profile of large transition-metal complexes, size reduced models were employed throughout this study that mimic both atomic electronic behaviour and molecular structure. Three specific optimisation models where used.

Model-opt: Geometry optimisations were performed by using the hybrid density functional B3LYP[28–31] in combination with a general basis set (termed GBS1) employing LANL2DZ[32,33] on tantalum and 6-31G(d)[34] on other atoms. Molecular structures were reduced in size such that both *t*Bu and Ar groups were replaced with H. Single-point energy calculations on these geometries were performed with B3LYP (and BP86[28,35], see the Supporting Information) and a larger basis set (termed GBS2, see the Supporting Information) on molybdenum, expanded to triple zeta with the inclusion of diffuse and f polarisation functions, and combined with 6-311+G(2d,p)[36] on other atoms. Final energies at the Model-Opt level are reported as B3LYP/GBS2//B3LYP/GBS1. This level of theory has proven to give accurate and reliable reaction geometries for three-coordinate transition-metal complexes.[5,18,21]

QM:QM and **QM:MM**: In those cases requiring inclusion of steric bulk, optimisations and some linear transit calculations have been carried out by using a two level ONIOM[37–39] method as incorporated in the Gaussian 03 program.[40] For the amide system and smaller components of the silox system the central metal, amides, silox and CO components were modelled with the above-mentioned B3LYP/GBS1, whereas the peripheral *t*Bu and Ph groups (Ar replaced with Ph on the amides) were modelled with B3LYP, but with the smaller 3-21G basis set.[34] This model is termed the QM:QM model. For the large-structure linear transits carried out in the silox system a further reduction in the level of theory was necessary and so the peripheral *t*Bu groups were modelled with the Universal Force Field (UFF) method.[41] This model is termed the QM:MM model. Except where noted all single-point energies of all QM:QM optimised structures were carried out by using B3LYP/GBS2.

All final geometries were optimised with unrestricted wavefunctions and reoptimisation was carried out in those cases in which wavefunction instabilities were observed. Five d-functions were used in the basis set throughout these calculations. Frequency calculations were performed with all structures characterised as minima or transition states based on the observed number of imaginary frequencies. All transition structures contained exactly one imaginary frequency and were linked to reactant, products or intermediates by using the intrinsic reaction coordinate calculations.[42] Except where noted, all energies reported in this publication include Gibbs free energy corrections taken from the lower level of theory (reported as ΔG_{298}). All minimum-energy crossing-point (MECP) calculations were carried out at the B3LYP/GBS2 level of theory by using the code provided by Dr. Jeremy Harvey,[43,44] and are uncorrected due to the absence of stationary points at the MECPs. All calculations were carried out with the Gaussian 03 set of programs.[40]

Results and Discussion

Validation of the B3LYP functional for transition-metal complexes has been performed in the past by our group[4,18] and others,[39,45–47] but to add justification to this analysis, the optimised geometries for [(silox)$_3$Ta–CC–Ta(silox)$_3$] calculated using the reduced Model-opt and full QM:QM ligand

systems were compared with the published X-ray crystal data.[25] The predicted and experimental geometries are almost identical in both cases, although the spin state of this dicarbide species requires additional analysis and is the subject of some discussion throughout the manuscript. These results and additional structural and energetic comparisons between the reduced model and full ligand system can be found in the Supporting Information and throughout the manuscript. Energetic comparisons using BP86/GBS2 applied to the geometries obtained using B3LYP/GBS1 have also been carried out. These results are available in the Supporting Information and closely match the mechanistic findings reported here using B3LYP/GBS2.

[(Silox)$_3$Ta−CCO] (6_S) Formation: Modelling the reaction of the three-coordinate tantalum silox complex $\mathbf{1}_S$ with CO centres around the formation and bonding interaction of the $\mathbf{1}_T$-CO adduct (Figure 1). Our calculations of the reactant at

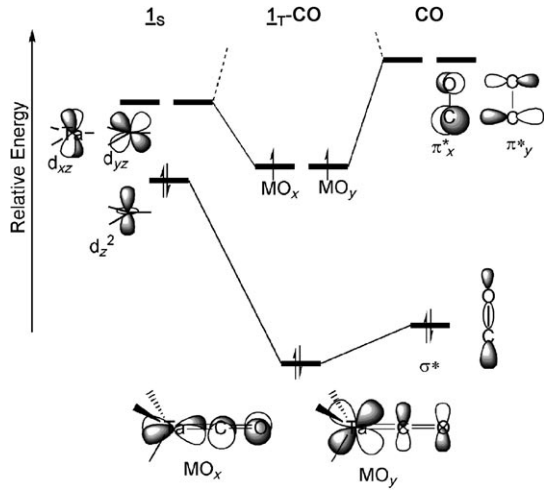

Figure 1. Illustration of the bonding interaction present in $\mathbf{1}_T$-CO [(silox)$_3$Ta−CO]

the Model-opt level of theory match experimental observations[24] of a C_3 trigonal [Ta(silox)$_3$] reactant ($\mathbf{1}_S$, see Figure 2) and confirm a diamagnetic state with a filled d_{z^2} orbital as the HOMO in the frontier orbital analysis. The filled d_{z^2} arrangement is a result of the strong π-donor ability of the silox ligands. As illustrated in Figure 1, the interaction with CO occurs through an overlap of the CO π* and the Ta d_{xz} (or d_{yz}) orbitals to form [(silox)$_3$Ta−CO] ($\mathbf{1}_S$-CO), which has a slightly distorted trigonal pyramidal structure with the (C bound) CO located at the apex (see Figure 2). The degeneracy of the tantalum d orbitals and Hund's rule forces a spin flip to single occupancy of the d orbitals and formation of the symmetric triplet structure $\mathbf{1}_T$-CO. This is confirmed from Model-opt calculations that have the triplet $\mathbf{1}_T$-CO 36.6 kJ mol^{-1} more stable than singlet $\mathbf{1}_S$-CO, and a minimum energy crossing point from singlet to triplet just

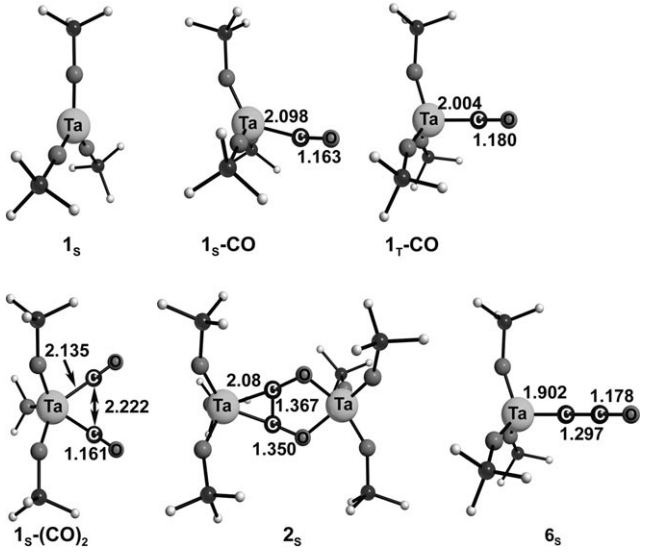

Figure 2. Model-opt geometries of selected silox species. All values in Angstroms.

2.3 kJ mol^{-1} above the singlet energy, indicating perhaps that the singlet species would be short lived if at all. This point is supported by a linear transit carried out on both spin surfaces at both the Model-opt and QM:QM levels of theory (see the Supporting Information). These transits also highlight a barrierless path to $\mathbf{1}_T$-CO from $\mathbf{1}_S$ + CO.

The bonding present in $\mathbf{1}_T$-CO is accompanied by the expected slight activation encountered with all end-on bound carbonyl groups (1.138 Å for CO and 1.180 Å for $\mathbf{1}_T$-CO). The silox group in this situation provides sufficient bulk to prevent reactant dimerisation, but allows enough space around the Ta centre for unhindered CO access. The overall reaction can be summarised as follows:

$$\mathbf{1}_S + CO \rightarrow \mathbf{1}_T\text{-CO} \qquad \Delta G = -26.8\ \text{kJ mol}^{-1} \tag{1}$$

Having established the presence of $\mathbf{1}_T$-CO, the pathway to ketenylidene $\mathbf{6}_S$ can now be considered. Given that the reacting mixture now contains three species $\mathbf{1}_S$, CO and $\mathbf{1}_T$-CO, there are statistically three new pathways available: addition of $\mathbf{1}_S$ to $\mathbf{1}_T$-CO, addition of CO to $\mathbf{1}_T$-CO or a combining of two $\mathbf{1}_T$-CO molecules. Each of these pathways requires close evaluation and the overall outcome is well illustrated in Scheme 2.

Calculations show that the pathway to the left in Scheme 2 is the energetically favoured one. It involves coordination of additional CO to form structure $\mathbf{1}_S$-(CO)$_2$ such that the two CO groups are in a *cis* position. This structure can then coordinate an additional reactant $\mathbf{1}_S$ to form a very stable intermediate $\mathbf{2}_S$, which we believe to be the uncharacterised red intermediate. Scission of one CO bond then gives the ketenylidene $\mathbf{6}_S$ through transition structure $\mathbf{2}_S$TS. Figure 2 displays the key Model-opt geometries and Figure 3 outlines the relative energy surface for this pathway.

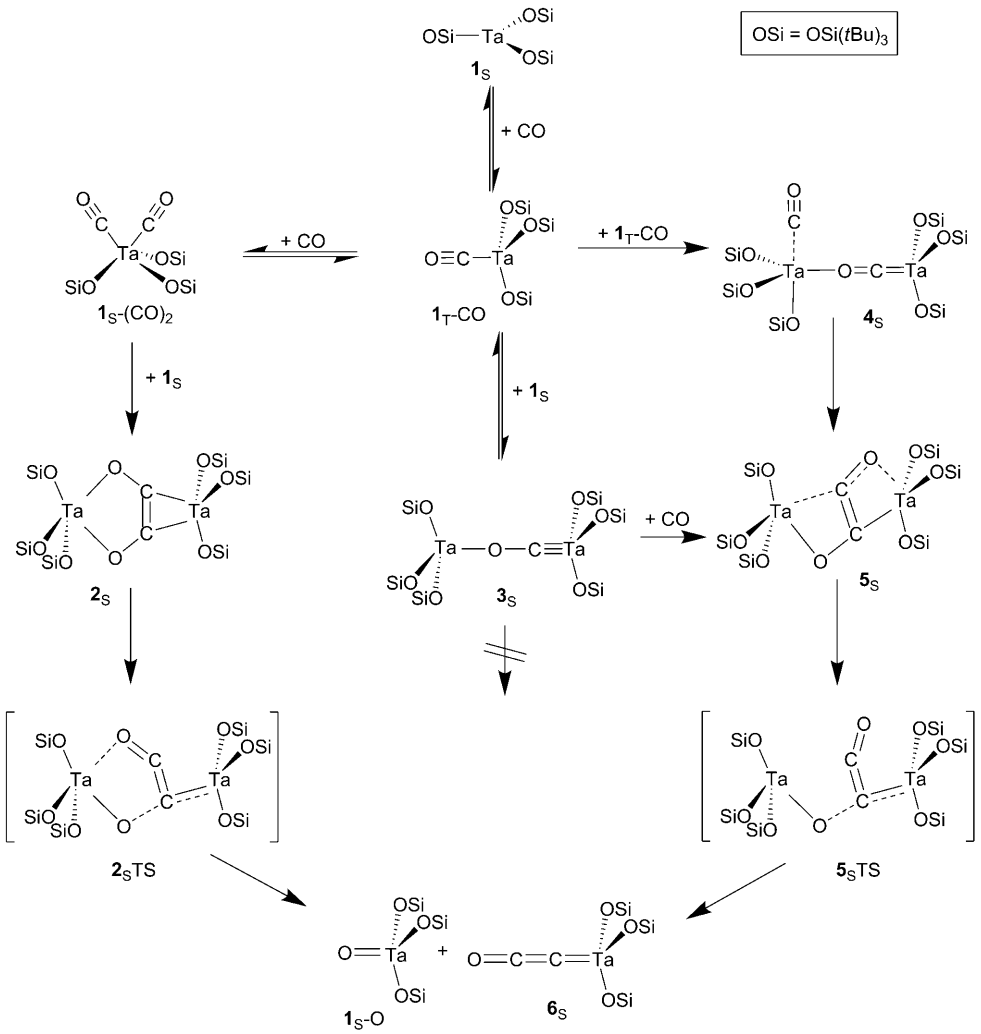

Scheme 2. Schematic diagram indicating the three potential pathways to formation of ketenylidene $\mathbf{6}_S$.

Prior to a closer analysis it is pertinent to review the experimental findings in regard to this unidentified red intermediate found on the path to $\mathbf{6}_S$. Experimentally,[24] the thermally unstable red precipitate was noted prior to formation of the [(silox)$_3$Ta–CCO] ketenylidene species ($\mathbf{6}_S$). Its characterisation was difficult due to its thermal instability. No solvent binding was evident in its structure, excess CO inhibits its formation, it does not dissociate CO, empirically it is believed to be [(silox)$_3$TaCO]$_2$, labelling experiments suggest the C=C double bond has formed and the absence of $\mathbf{1}_S$-O suggests that both CO bonds have not been completely severed. At a glance our proposed $\mathbf{2}_S$ adheres to all of these observations but now consider the pathway outlined in Scheme 2 more closely.

Starting from $\mathbf{1}_S$, two molecules of CO can coordinate directly on the same spin surface without a barrier to form $\mathbf{1}_S$-(CO)$_2$. This may be unlikely since the first CO addition to $\mathbf{1}_S$ will instantly spin flip to the triplet $\mathbf{1}_T$-CO (see above) and so the pathway starting from $\mathbf{1}_T$-CO should be explored. As outlined in Figure 3, additional CO coordinates to $\mathbf{1}_T$-CO in the *cis* orientation, initially in the triplet electronic state ($\mathbf{1}_T$-(CO)$_2$), before passing to the singlet ($\mathbf{1}_S$-(CO)$_2$). The uncorrected electronic energies of these last two species are identical with a weakly attached apical CO group on the trigonal bipyramidal triplet resulting in a slight entropic difference. The MECP linking the two structures is calculated to be just 14.9 kJ mol^{-1} above the triplet surface.

One might expect a *trans* isomer of $\mathbf{1}_T$-(CO)$_2$ (or $\mathbf{1}_S$-(CO)$_2$) to be more stable as postulated in the experimental evaluation.[24] This assumption was based on the single carbonyl infrared stretching frequency of the THF-$\mathbf{1}_T$-CO adduct[48] shifting from 1840 to 1870 cm^{-1} in the presence of additional CO. Our calculations indicate that the *trans* isomer is some 22.3 kJ mol^{-1} less stable than the *cis* orientation and that its structure is trigonal bipyramidal such that one CO group is loosely bound. This structure does not support the experimental findings of one CO environment. However, the more stable singlet *cis* isomer possesses C_S

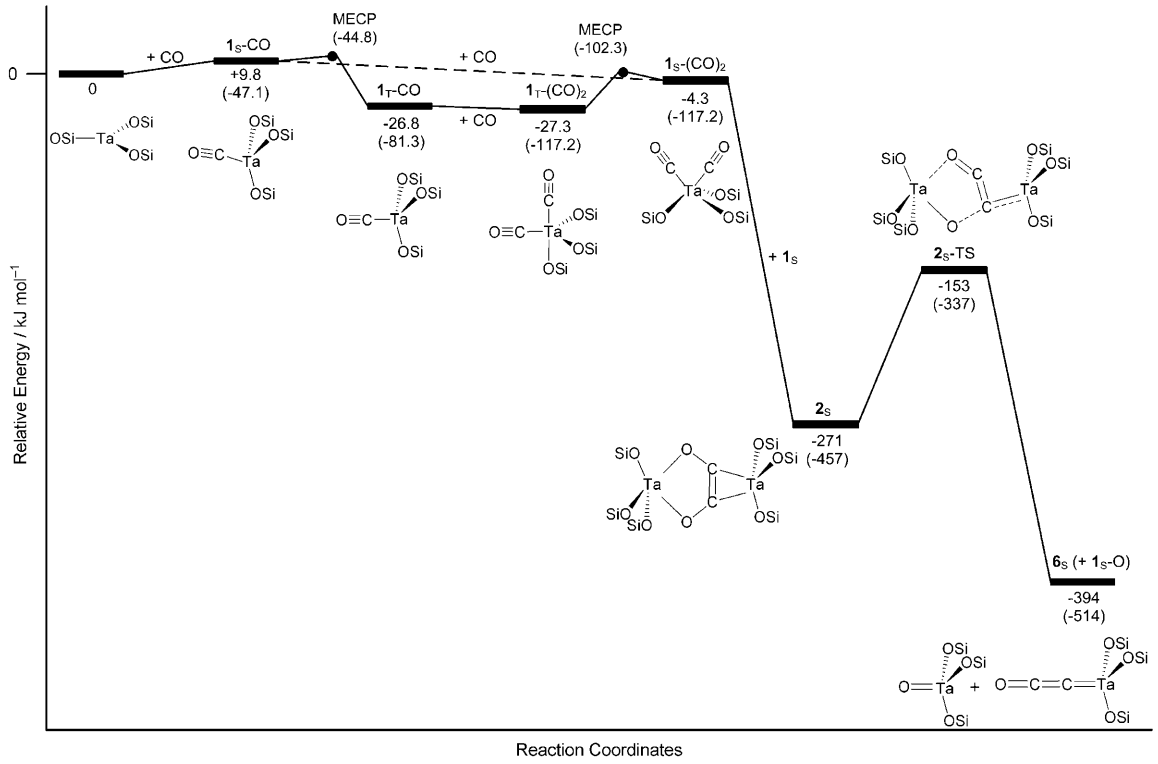

Figure 3. Relative energy surface for the formation of ketenylidene $\mathbf{6}_S$ from $\mathbf{1}_S$ and CO via intermediate $\mathbf{2}_S$. Figure constructed relative to Gibbs free energies (in normal type). Values in parentheses are uncorrected electronic energies. All values in kJ mol^{-1}.

symmetry and is the only conformer that has just the single CO environment. Illustrations of these and other structures are available in the Supporting Information.

The bonding arrangement in $\mathbf{1}_S$-$(CO)_2$ is surprisingly simple as shown in the molecular orbital diagrams in Figure 4. The HOMO illustrates the symmetric 3-centre 2-electron bond between the tantalum d orbital and two π*orbitals of the CO groups. The LUMO indicates that if some electron density was available a pyramidal structure might be preferred or perhaps if fully occupied a C–C bond might form.[49] The overall natural bond orbital (NBO) electron donation from $[Ta(silox)_3]$ to the two CO groups is only a modest 0.16 e indicating the C–C bond formation is unlikely to occur in this moiety, a fact confirmed by failed optimisations involving a preformed C–C bond that always reverted to the current structure displayed for $\mathbf{1}_S$-$(CO)_2$.

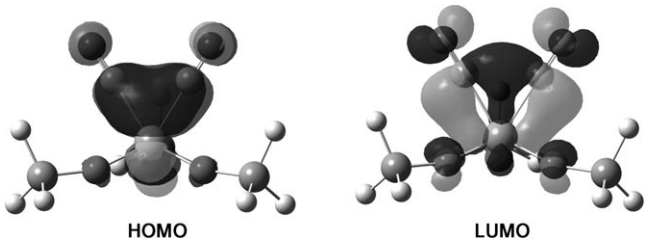

Figure 4. HOMO and LUMO molecular orbitals for $\mathbf{1}_S$-$(CO)_2$.

Addition of further CO to $\mathbf{1}_S$-$(CO)_2$ produces no energetically favourable products, but extra $\mathbf{1}_S$ reactant provides the pathway to intermediate $\mathbf{2}_S$. The $\mathbf{1}_S$ structure bonds through the easily accessible π* CO orbitals and the d orbitals of the incoming tantalum. This conveniently supplies $\mathbf{1}_S$-$(CO)_2$ with extra electron density, thus filling the orbital responsible for the C–C bond and bringing the two carbon atoms closer together. This net transfer of electron density is seen in the NBO analysis in which the electron donation from the two $[Ta(silox)_3]$ groups to the $(CO)_2$ has increased to −1.364 e (from 0.16 e in $\mathbf{1}_S$-$(CO)_2$). The bonding arrangement is now akin to having a non-linear ethene 1,2-dione wedged between two $[Ta(silox)_3]$ groups.

It should be noted that an equally likely pathway to $\mathbf{2}_S$ could occur initially on the triplet surface prior to spin pairing and formation of the more stable singlet (i.e., $\mathbf{1}_S+\mathbf{1}_T$-$(CO)_2 \rightarrow \mathbf{2}_T \rightarrow \mathbf{2}_S$). At the Model-opt level of theory this pathway has almost identical energetic barriers to that described above, however, we believe it is not the preferred pathway, since the transition structure undergoes significant distortion during the C–C bond formation. To calculate the destabilisation due to steric distortion using QM:QM is currently beyond our computational budget, but for interested readers the Model-opt structures and relative energy surface are available in the Supporting Information.

The molecular orbital interaction present in intermediate $\mathbf{2}_S$ is a little more involved than that of $\mathbf{1}_T$-CO and $\mathbf{1}_S$-$(CO)_2$.

The π bonding interaction between the carbon and oxygen atoms of the central $\mathbf{2}_S$ dione presents us with a series of eight symmetry-adapted orbitals. As indicated in Figure 5, the four lower-lying orbitals remain independent of the metal interaction as does π4′. The π3 orbital has a minor interaction with the symmetry adapted d_{z^2} orbital, but it is the high lying π4 and π3′ antibonding orbitals that provide the most important component of this scheme. Both π4 and π3′ are nicely stabilised by the interaction with the $d_{xz}+d_{xz}$ and $d_{yz}+d_{yz}$ Ta orbitals respectively, thus creating low-lying orbitals that act as a potential well for metal electron back donation, which creates the stable intermediate $\mathbf{2}_S$. The structure formed by this interesting interaction is one of a stable C–C bond, strengthened Ta–C bonds and, perhaps most importantly, the creation of Ta–O bonds and highly activated C–O bonds, now at 1.37 Å (from 1.16 Å in $\mathbf{1}_S$-$(CO)_2$). It is this latter component that allows the reaction to progress to the isolatable ketenylidene intermediate $\mathbf{6}_S$. Diagrams of the structures created can be seen in Figure 2.

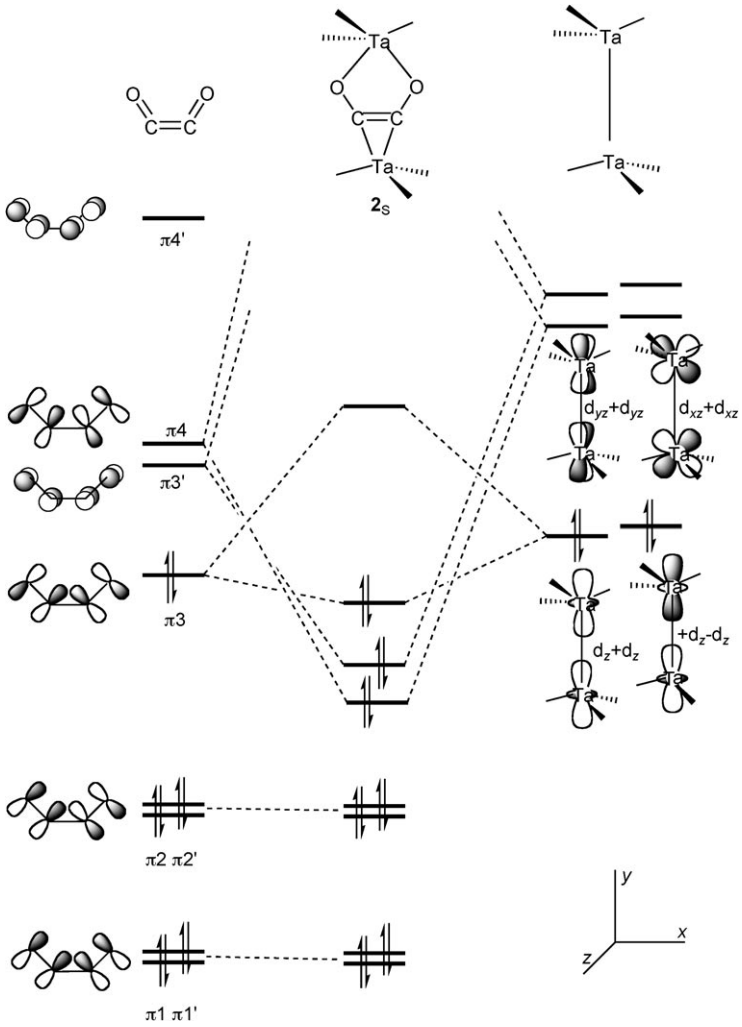

Figure 5. Abbreviated molecular orbital diagram of $\mathbf{2}_S$ $[(silox)_3Ta{-}CO]_2$. Note π1′ and π2' are not displayed as are several of the symmetry adapted tantalum d orbitals.

Having established that electron donation from the metal centres is responsible for this intermediate $\mathbf{2}_S$, one might consider the effect of decreasing or even increasing the electron-donating ability of the second incoming $[Ta(silox)_3]$ group. This concept can be easily tested by calculating the optimum geometry for the intermediate in which the second (oxygen-bonded) Ta is replaced with electron-deficient metals, such as d^1 hafnium or d^0 lanthanum, or, perhaps, electron-rich metals, such as d^3 tungsten or d^4 rhenium. If our electron donation postulate is correct, we should see reduced interaction with the electron-deficient metals[50] and no change to the electron-rich metals. Figure 6 outlines the geometries of these species and illustrates the importance of having sufficient electron density available in the second metal to back donate and create the $\mathbf{2}_S$ structure. The lanthanum analogue, which has no available electrons, shows complete dissociation of the second group, whereas hafnium, with just one available d electron, produces a weak C–C bond, less activated C–O bonds and weak binding to the oxygen atoms. Little difference is observed for the electron-rich tungsten or rhenium analogues.[51]

Although beyond the scope of this manuscript, these analogous metal results tend to imply that a mixed-metal $[(silox)_3Ta{-}(CO)_2{-}W(silox)_3]$ intermediate might be synthetically possible. Given that $[W(silox)_3]$ has recently been synthesised,[27] its addition under controlled temperature and stoichiometry to $\mathbf{1}_S$-$(CO)_2$ may provide a mixed-metal inter-

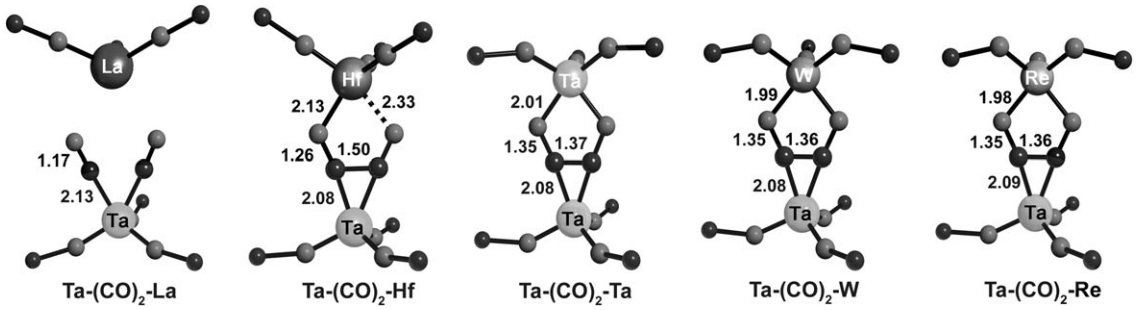

Figure 6. Moldraw representations of $[(SiO)_3Ta{-}(CO)_2{-}La(OSi)_3]$, $[(SiO)_3Ta{-}(CO)_2{-}Hf(OSi)_3]$, $[(SiO)_3Ta{-}(CO)_2{-}Ta(OSi)_3]$, $[(SiO)_3Ta{-}(CO)_2{-}W(OSi)_3]$ and $[(SiO)_3Ta{-}(CO)_2{-}Re(OSi)_3]$. Geometries calculated at the Model-opt level of theory. Hydrogen atoms are omitted from diagrams and all dimensions are in Å.

mediate that produces the tantalum ketenylidene $\mathbf{6}_S$ and [(silox)$_3$W–O]. Our uncorrected GBS1 Model-opt calculations indicate that a similar exothermicity exists for the formation of this Ta/W mixed-metal intermediate (see the Supporting Information).

The alternate pathway to the formation of ketenylidene $\mathbf{6}_S$, as displayed in Scheme 2, involves coordination of $\mathbf{1}_T$-CO to either $\mathbf{1}_S$ or to another $\mathbf{1}_T$-CO. Both of these pathways have been explored and are interlinked, with both leading to the same intermediate ($\mathbf{5}_S$) prior to C–O scission through transition structure $\mathbf{5}_S$TS, and formation of $\mathbf{6}_S$ plus $\mathbf{1}_S$-O (see Figure 7). The $\mathbf{5}_S$ intermediate is again akin to having an ethene 1,2-dione wedged between two [Ta(silox)$_3$] groups, but in this instance the dione has a zigzag arrangement in which two distinct environments exist for the C–O bonds. The (NBO-calculated) electron back donation from the two metal centres to the dione is again significant at 1.417 e and the molecular orbital analysis is surprisingly similar to that for $\mathbf{2}_S$ (in Figure 5 and also the Supporting Information) with the exception being the $\pi 4'$ orbital interacting with the metal to create the LUMO. This has no overall effect on the structure at hand (see Figure 8), it still possess sufficient electron density to create the C–C bond and has a highly activated CO bond.[52]

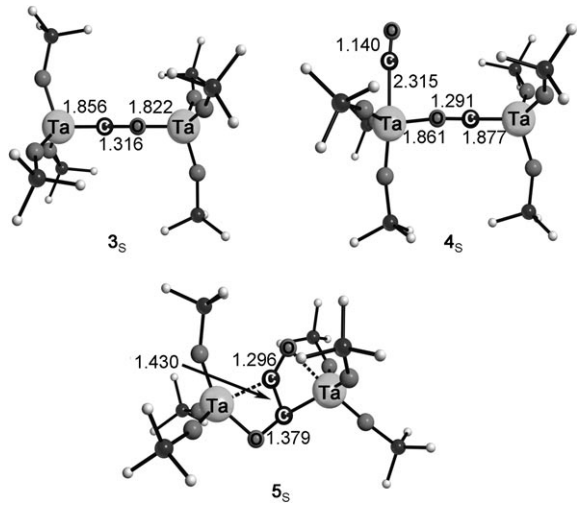

Figure 8. Model-opt geometries of species $\mathbf{3}_S$, $\mathbf{4}_S$ and $\mathbf{5}_S$. All values in Å.

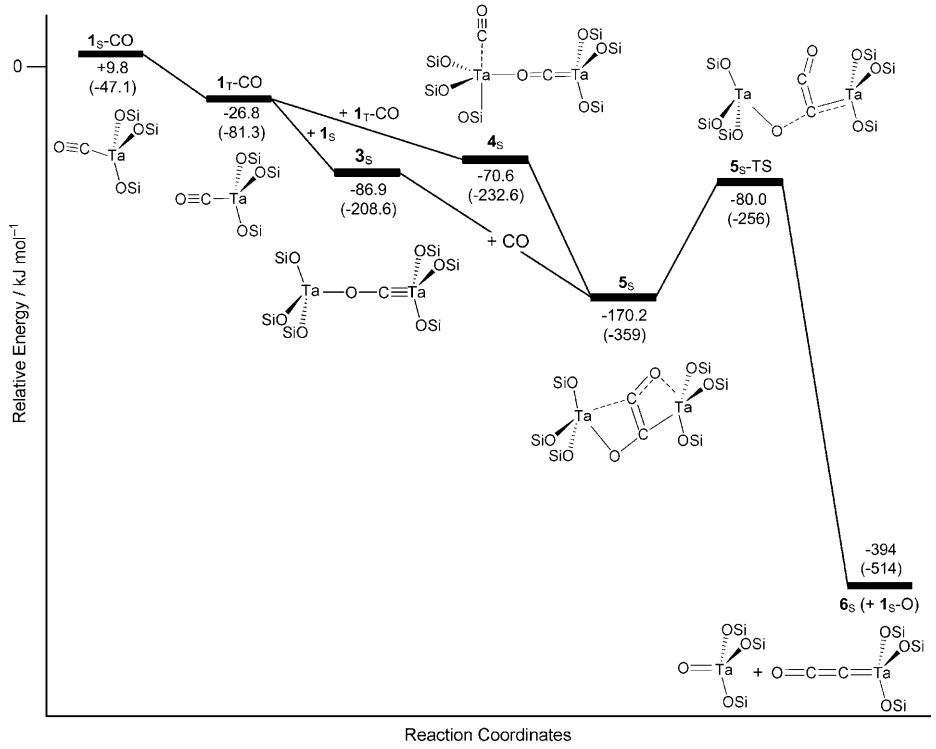

Figure 7. Simplified relative energy surface for the formation of (possible) intermediate $\mathbf{5}_S$ prior to C–O scission to create $\mathbf{6}_S$ and $\mathbf{1}_S$-O. Calculations performed at the Model-opt level of theory. Figure constructed relative to Gibbs free energies (in normal type). Values in parentheses are uncorrected electronic energies. All values in kJ mol^{-1}.

The formation of structure $\mathbf{5}_S$ is complicated somewhat by the potential for numerous spin crossings and so a simplified relative energy surface has been displayed in Figure 7. The full diagrams are available in the Supporting Information, but overall the energy of the spin crossings does not affect the potential for intermediate formation or CO scission. The first pathway to $\mathbf{5}_S$ involves $\mathbf{1}_T$-CO combining with an additional reactant to form $\mathbf{3}_S$, which can further react with additional CO to form $\mathbf{5}_S$. The formation of $\mathbf{3}_S$ is without barrier and the stability afforded to the structure is due to the electron donation from the second Ta atom to the two singly occupied degenerate orbitals of $\mathbf{1}_T$-CO. In fact, the molecular orbital arrangement of $\mathbf{3}_S$ is remarkably similar to that displayed in Figure 1 for $\mathbf{1}_T$-CO but now the two degenerate HOMOs are fully occupied. NBO analyses support this concept whereby the overall charge on the central CO has increased from 0.22 e in $\mathbf{1}_T$-CO to 0.89 e in $\mathbf{3}_S$. In essence the bonding π orbitals of the central Ta–CO–Ta are saturated. Interestingly, this structure will not cleave CO. No barrier exists to the scission, but the products $\mathbf{1}_S$-O and $\mathbf{1}_S$-C lie +79.2 kJ mol^{-1} above $\mathbf{3}_S$ making C-O cleavage thermodynamically unlikely.

Given its saturated nature, it is no surprise to find that an incoming CO will not interact with the two metal centres of

$\mathbf{3}_S$. No electron density is available for back donation from the metal centres, but the empty π* orbitals of the incoming CO can interact with the electron-rich bonded CO group, thus creating $\mathbf{5}_S$ without barrier. We have, up to this point, neglected to discuss steric implications on most of the interactions. It turns out that the silox steric bulk has little effect on the reaction outcomes involving $\mathbf{1}_S$, since its large open structure provides ample access to small molecules from above the 3-coordinate plane. This is not the case for the $\mathbf{3}_S$+CO interaction however, since the silox framework creates a cage like structure that encircles the central Ta−CO−Ta core, ultimately creating an energy barrier to attack. To accurately measure the energy required to penetrate this steric enclosure is difficult for molecules of this size. Our measurements obtained by using a QM:MM linear transit place its value at around $+15\ kJ\,mol^{-1}$, whereas a constrained optimisation at the QM:QM level of theory would suggest a barrier of greater than $+59\ kJ\,mol^{-1}$ to be more realistic (see the Supporting Information for full ligand and space-filled diagrams plus energies). These values are approximate, but as a general comment, it is sufficient to say that a not-insurmountable steric barrier exists to CO coordination with $\mathbf{3}_S$ and, thus, formation of $\mathbf{5}_S$.

The second pathway to the formation of $\mathbf{5}_S$ in Figure 7 and Scheme 2 involves combining two $\mathbf{1}_T$-CO adducts in a head-to-head fashion (Ta−CO+OC−Ta). This leads to the formation of $\mathbf{4}_S$, which has a partially dissociated CO group. This dissociation is a result of the stable arrangement of the Ta−CO−Ta structure ($\mathbf{3}_S$) as discussed above. The energy to completely sever this loosely attached CO group from $\mathbf{4}_S$ is less than the entropic effect of dissociation, and so the CO will detach without barrier (see the Supporting Information). One might expect the now free CO to translate onto the centrally bound carbon. Unfortunately, at the Model-opt level of theory this does not occur naturally and requires user intervention to move the free CO into a more desirable position for bonding. However, the steric cage discussed above for $\mathbf{3}_S$, again becomes an important consideration for $\mathbf{4}_S$. Just as $\mathbf{3}_S$ had a barrier preventing CO interaction, $\mathbf{4}_S$ has a containment barrier to CO loss. At the QM:MM level of theory the presence of the silox bulk pushes the dissociated CO towards the bound carbon making the transit to $\mathbf{5}_S$ highly likely. To use the figures quoted above, a barrier of greater than $+59\ kJ\,mol^{-1}$ must be overcome to prevent rearrangement of $\mathbf{4}_S$ to $\mathbf{5}_S$. This steric arrangement also highlights the reason why a head-to-head interaction must be considered, since the head-to-tail (i.e., Ta−CO+Ta−CO) case results in formation of $\mathbf{3}_S$ and unbound CO, which is located outside the steric cage.

Before discussion of the dicarbide formation, some additional comment needs to be made in regard to the formation of $\mathbf{4}_S$ and $\mathbf{5}_S$. Firstly, our calculations do not support a direct formation of $\mathbf{5}_S$ from two incoming $\mathbf{1}_S$-CO (or $\mathbf{1}_T$-CO) molecules. Every effort to create a direct C−C coupling pathway was always preceded by O−Ta bond formation as in $\mathbf{4}_S$. Secondly, the reaction $2(\mathbf{1}_S\text{-CO})\rightarrow\mathbf{4}_S$ on the singlet surface at the Model-opt level of theory is without barrier. But a barrier of $+47\ kJ\,mol^{-1}$ was noted when steric bulk was included in a QM:MM linear transit and a more realistic value of $+31.5\ kJ\,mol^{-1}$ was found by using a constrained optimisation at the QM:QM level of theory (see the Supporting Information for both transit and constrained optimisation). And finally, one might expect $\mathbf{4}_S$ or even $\mathbf{5}_S$ to rearrange to the energetically favoured $\mathbf{2}_S$ before progressing to ketenylidene $\mathbf{6}_S$. A pathway for rotation of the dissociated CO to form $\mathbf{6}_S$ could not be found at the Model-opt or QM:MM levels of theory, with all optimisations leading to $\mathbf{5}_S$. Of course the CO could rotate once $\mathbf{5}_S$ has formed, thus creating $\mathbf{2}_S$, but this rotation faces a barrier of $+107.1\ kJ\,mol^{-1}$, which is higher than that required to form $\mathbf{6}_S$ directly by C−O scission(see structure $\mathbf{5}_S\mathbf{2}_S$TS in the Supporting Information).

Formation of dicarbide [(silox)$_3$Ta−CC−Ta(silox)$_3$]($\mathbf{9}_S$) from ketenylidene $\mathbf{6}_S$: Once formed, ketenylidene ($\mathbf{6}_S$) is known to react experimentally with additional reactant ($\mathbf{1}_S$) to form dicarbide [(silox)$_3$Ta−CC−Ta(silox)$_3$] ($\mathbf{9}_S$), which is expected to have a singlet electronic state. Neithamer et al.,[24] postulated a mechanism whereby the additional $\mathbf{1}_S$ reactant deoxygenates the ketenylidene via an intermediate [(silox)$_3$Ta=C=C−O−Ta(silox)$_3$] ($\mathbf{7}_S$) producing a transient vinylidene [(silox)$_3$Ta=C=C:] ($\mathbf{8}_S$), which is scavenged by another reactant to form the dicarbide end product ($\mathbf{9}_S$). This scheme is replicated by our Model-opt calculations and the structures obtained are illustrated in Figure 9.

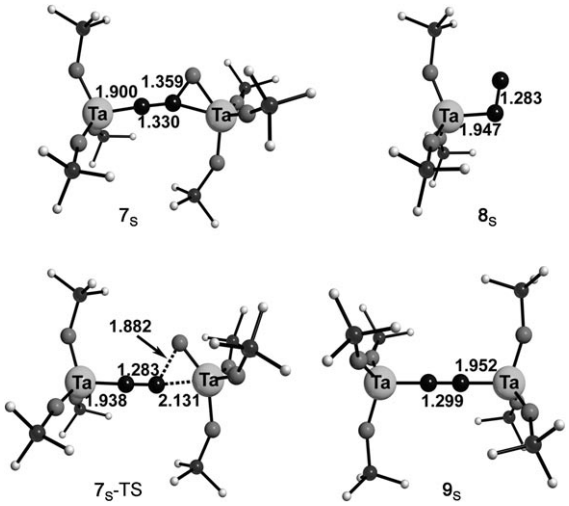

Figure 9. Model-opt geometries of species $\mathbf{7}_S$, $\mathbf{7}_S$TS, $\mathbf{8}_S$ and $\mathbf{9}_S$. All values in Å.

The additional reactant $\mathbf{1}_S$ forms a side-on bonding arrangement to the apical CO of $\mathbf{6}_S$ through an empty CCO π*orbital to form [(silox)$_3$Ta-C=C-O-Ta(silox)$_3$] ($\mathbf{7}_S$). This interaction, centred on the more electronegative apical oxygen, provides the necessary electron density to weaken the CO bond and allow its scission. This can be seen in Figure 9 in which the CO bond length in $\mathbf{7}_S$ has increased to

1.359 Å from 1.178 Å found in $\mathbf{6}_S$ (Figure 2). Removal of the oxygen occurs through transition structure $\mathbf{7}_S$TS leaving the reactive vinylidene transient species $\mathbf{8}_S$, which forms the dicarbide $\mathbf{9}_S$ (or $\mathbf{9}_T$) after accepting another reactant. The relative energy surface of this interaction can be seen in Figure 10.

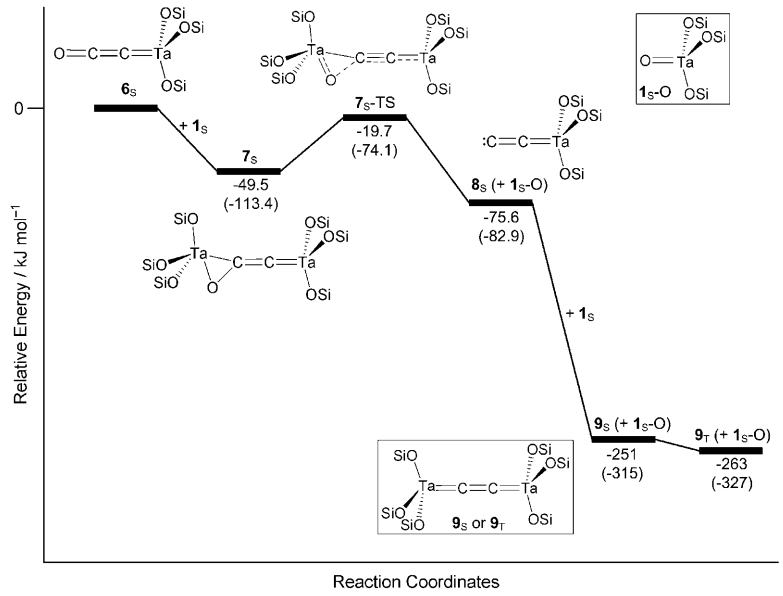

Figure 10. Relative energy surface for the interaction between ketenylidene ($\mathbf{6}_S$) and [Ta(silox)$_3$] ($\mathbf{1}_S$) at the Model-opt level of theory. Figure constructed relative to Gibbs free energies (in normal type). Values in parentheses are uncorrected electronic energies. All values in kJ mol^{-1}.

Some interesting observations can be made here in addition to those outlined in the original manuscript of Neithamer et al.[24] Firstly, the C–O bond is cleaved in $\mathbf{6}_S$, whereas for the similar $\mathbf{3}_S$, with one less carbon, the C–O bond is not, despite the bond being similarly activated. In simple terms, a CO structure is not cleaved but a CCO is cleaved. This observation poses the question, why does the presence of an extra carbon allow the C–O bond to be broken and what might occur if the central arrangement was altered to say CCCO or even CCCCO? Would the C–O bond of an extended species be cleaved if reacted with additional $\mathbf{1}_S$? Table 1 considers the latter component of this question and outlines our calculations in regard to increasing the central C_nO structure (in which $n=1$, 2, 3, 4, etc.). These findings also help explain the cleavage of (or lack there of) CO in structures of the form [(silox)$_3$Ta–C_nO].

Table 1. Gibbs free energy of reaction at the Model-opt level of theory. [Ta(silox)$_3$] replaced with Ta. All values taken from structures at their lowest-energy spin state.

n	Ta–C_nO + $\mathbf{1}_S$ → Ta–C_nO–Ta	Ta–C_nO–Ta → Ta–C_n + $\mathbf{1}_S$-O
1	−60.1 kJ mol^{-1}	+79.2 kJ mol^{-1}
2	−49.5 kJ mol^{-1}	−26.1 kJ mol^{-1}
3	−277.2 kJ mol^{-1}	+104.5 kJ mol^{-1}
4	−73.7 kJ mol^{-1}	−11.8 kJ mol^{-1}

The data indicates that formation of a dinuclear Ta–C_nO–Ta is exergonic in all cases. The subsequent reaction in which C–O is cleaved is unfavourable for $n=1$ and 3 (odd), but favourable for $n=2$ and 4 (even). This pattern can be explained in simplistic terms. When n is odd, the Ta–C_nO structure is in a triplet spin state and can be considered electronically unsaturated. This is illustrated in Figure 1 for the $n=1$ case. It can readily receive electron density from an incoming reactant filling MO_x and MO_y in Figure 1, to form a stable electronically saturated, Ta–C_nO–Ta structure from which C–O cleavage is unlikely. However, when n is even the Ta–C_nO complex, with a singlet state, is already electronically saturated or specifically MO_x and MO_y in Figure 1 are full. Electron donation from an additional reactant into the antibonding orbitals will then have little stabilising effect, making an unstable intermediate and allowing C–O cleavage to form a more stable structure, such as Ta–C_n (+O–Ta). The "odd" case creates a stable intermediate, whereas the "even" case does not.

The second observation to be made is in regard to the structure of $\mathbf{8}_S$. The bonding analysis in $\mathbf{8}_S$ has been covered elsewhere,[24] but Figure 9 shows the structure in a strange bent bonding arrangement between the two carbon atoms and the metal centre. For simplicity, throughout this manuscript we have represented $\mathbf{8}_S$ with a linear Ta=C=C: axis, but this bent structure would perhaps be better represented with a charge separation between the metal and the α-carbon atom. This bent arrangement, which has the Ta d–$C_2\pi$ orbitals as non-degenerate, is energetically favourable by only 13 kJ mol^{-1} compared with a linear Ta–C–C arrangement at the Model-opt level of theory, whereas QM:QM has identical energies for the linear and bent arrangements. At this low energetic stability the bent orientation is unlikely to be fully maintained, but its presence, along with the steric hindrance provided by the silox groups, might provide reduced accessibility to a trapping species and may help explain why this vinylidene species has not been trapped experimentally.

Finally, the spin state of the dicarbide $\mathbf{9}_S$ was difficult to determine experimentally.[24] Our calculations at the Model-opt level of theory place the energy of the triplet just 12.4 kJ mol^{-1} lower than the singlet. Structurally both are

identical and no apparent distortion is present in the linear Ta–CC–Ta core to favour the singlet. Since the Model-opt calculations show no structural difference it can be assumed that steric bulk must play a part in the preferred magnetic state. Structural determination of both the triplet and singlet at the QM:QM level of theory again shows both to be almost identical with the only discernable difference being the slight distortion (4.2°) to the Ta–CC–Ta linear core in the singlet. Accurate energetic determination of structures this size is currently beyond our means, but the QM:QM optimised energies show the triplet to again be lower in energy, this time by around 29 kJ mol^{-1}(see the Supporting Information). This is certainly an approximate value, but it would be reasonable to conclude that the singlet and triplet dicarbides ($\mathbf{9}_S$ and $\mathbf{9}_T$) are of comparable energies. The analysis of the dicarbide is continued in the following section in which a comparison will be made with the analogous amide dicarbide structures.

Analogous amide [Ta(N(*t*Bu)Ph)$_3$]+CO reaction: Having established the reaction mechanism for the larger [Ta(silox)$_3$]+CO system, the concept of applying this reaction sequence to the Laplaza–Cummins three coordinate amide system[53] will now be considered. The difference between the two systems would at first appear to be solely steric in nature, since the silox system has additional space around the central metal core provided by the bridging oxygen atoms. But it should be remembered that the tri-amide system has this unique ability to rotate at least one amide group,[8,10,17,18] thus increasing electron density to the metal and altering the steric environment of the species. Unfortunately, the electronic stability afforded by amide rotation and steric bulk are closely linked as found in our previous study of the molybdenum tri-amide system[4,10] and, hence some QM:QM optimisations on structures will be necessary here.

As with the silox system, the important steps in the reaction occur in the initial adduct and the pathway to formation of an amide ketenylidene species, since this is the necessary precursor to the dicarbide dimer formation. Given that all of the reaction coordinates have been constructed for the silox system it should be a simple process of creating analogous model molecules replacing silox with amides. This proves to be the case when using our Model-opt theory. Figure 11 provides a graphical overview of the reaction relative energy surface, while Figure 12 illustrates the geometries. Figure 11 is the amide equivalent of Figure 3 and Figure 10 combined of the silox system. Tabulated energetic values are available in Table 2 along with a direct comparison with the calculated silox system.

Figure 11 suggests that the three coordinate amide reaction should progress identically to a tantalum amide dicar-

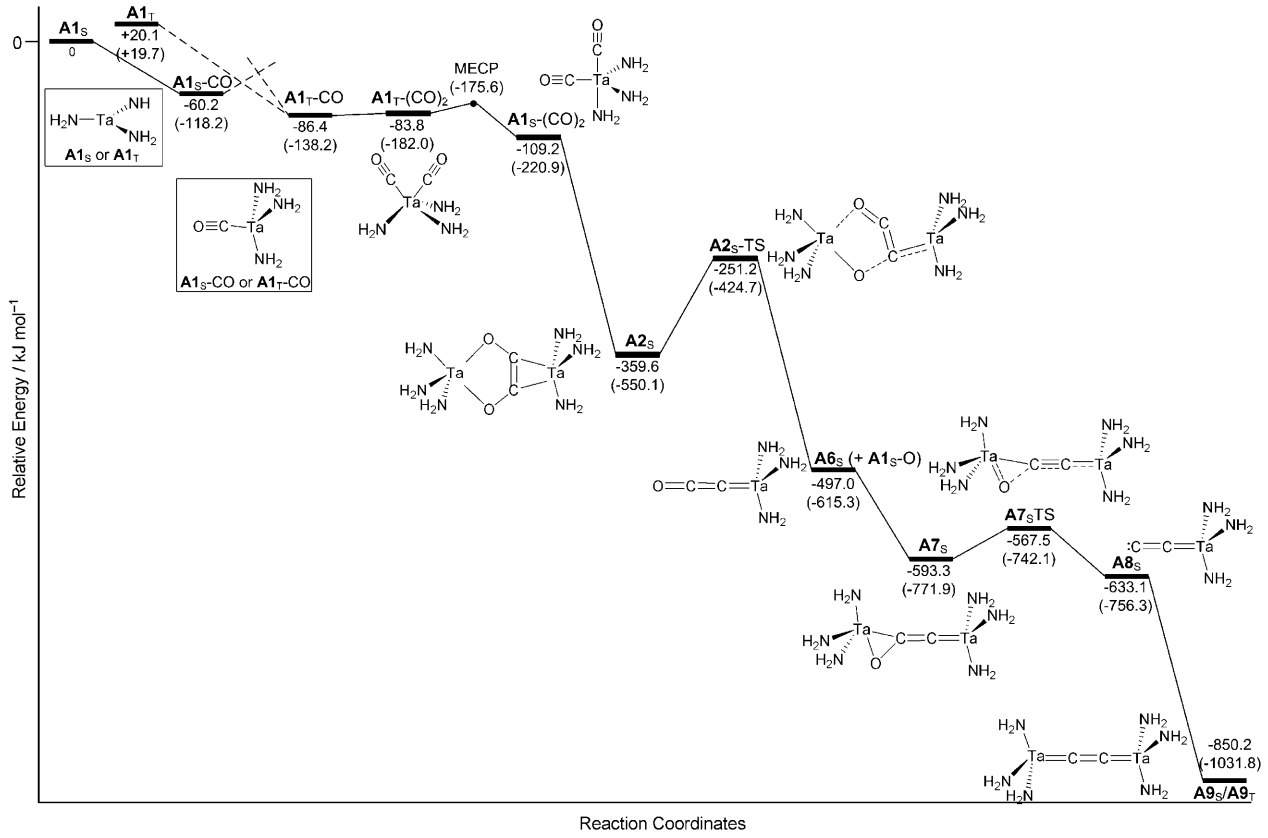

Figure 11. Relative energy surface for the [Ta(NH$_2$)$_3$]+CO reaction at the Model-opt level of theory. Figure constructed relative to Gibbs free energies (in normal type). Values in parentheses are uncorrected electronic energies. All values in kJ mol^{-1}.

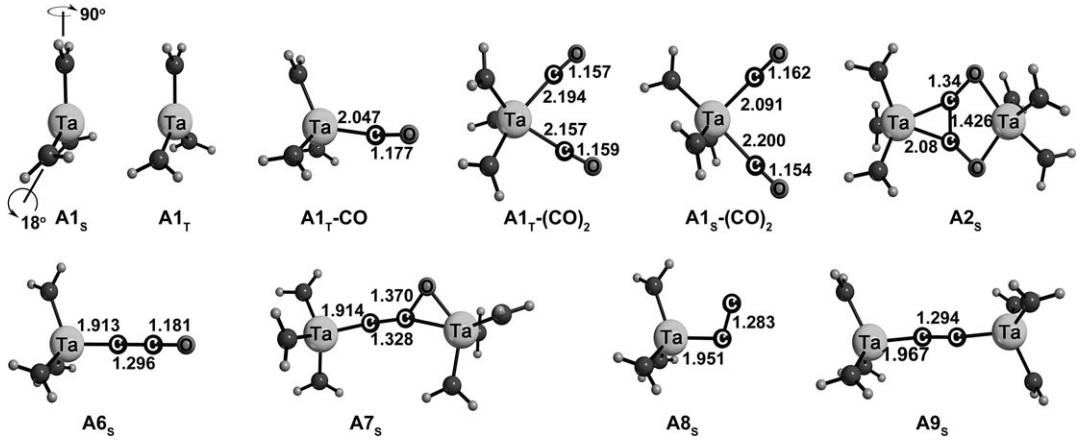

Figure 12. Model-opt geometries of selected amide species. All values in Å.

bide ($\mathbf{A9}_S$ or $\mathbf{A9}_T$) via the ketenylidene intermediate ($\mathbf{A6}_S$). A short lived intermediate at $\mathbf{A2}_S$ may also be observed. In fact, the amide system shows greater stability of all species relative to the reactants when compared with the silox system. This is particularly evident from the initial adduct $\mathbf{A1}_T$-CO, which is more stable than the silox analogue by 60 kJ mol^{-1}. As found by our group previously,[17] this additional stability is directly related to the ability of the amide groups to rotate, thus increasing the electron donation to the metal. For example, the NBO charge on the Ta atom in $\mathbf{A1}_T$-CO is +1.182, whereas for the silox equivalent it is +1.553. This comparison can be extended to every species throughout the reaction profile and in every case the amide metal carries more electron density compared with its silox equivalent (see the Supporting Information) at the Model-opt level of theory.

There are also numerous subtle differences and similarities in the profile outlined in Figure 11 (and the structures displayed in Figure 12) with those of the silox system. The list includes, the seemingly pointless inclusion of the triplet reactant in Figure 11, the reversal in structure and energy of $\mathbf{A1}_S$-$(CO)_2$ and $\mathbf{A1}_T$-$(CO)_2$, the splayed O-C-C-O angle of the central dione in $\mathbf{A2}_S$ compared with $\mathbf{2}_S$, the trigonal bipyramidal structure to the second Ta in $\mathbf{A2}_S$, the same bent tantalum dicarbide core in both $\mathbf{8}_S$ and $\mathbf{A8}_S$, and the almost identical energies of the singlet and triplet dicarbide end products $\mathbf{A9}_S$ and $\mathbf{A9}_T$. This list could also include the alternate pathways via $\mathbf{A3}_S$ or $\mathbf{A5}_S$, which are not included in the above diagrams. Unfortunately, the analysis of these interesting notes is complicated somewhat by the steric influence of the tightly bound phenyl (or aryl) and *tert*-butyl groups. Detailed analysis of intricacies such as these are covered in other publications,[4,8,10,13,17] but it would be remiss not to highlight some of those listed above that are specific to the proposed tantalum amide reaction sequence. In summary terms, Table 2 outlines the energetics of the species with and without steric consideration and as a comparison the analogous silox results are included.

The top of Table 2 highlights the first point. Steric inclusion at the QM:QM level of theory finds the triplet amide reactant $\mathbf{A1}_T$ to be more stable that the singlet $\mathbf{A1}_S$ and explains the presence of $\mathbf{A1}_T$ in Figure 11. The Model-opt level

Table 2. Model-opt and QM:QM energies of the proposed tantalum amide system. Silox energies included for comparison. Values in normal script are Gibbs corrected and those in parenthesis are uncorrected. All energies in kJ mol^{-1}.

	Amide system		Silox system	
Structure	Model-opt energy relative to $\mathbf{A1}_S$	QM:QM energy relative to $\mathbf{A1}_S$	Model-opt energy relative to $\mathbf{1}_S$	QM:QM energy relative to $\mathbf{1}_S$
$\mathbf{A1}_S$	0	0	0	0
$\mathbf{A1}_T$	+20.1 (+19.7)	−21.4 (−15.2)	+74.5 (+75.6)	+16.3 (+25.4)
$\mathbf{A1}_T$-CO	−86.4 (−138.2)	−102.4 (−156.0)	−26.8 (−81.3)	−24.6 (−66.6)
$\mathbf{A1}_T$-$(CO)_2$	−83.8 (−182.0)	−20.0 (−135.5)	−27.3 (−117.2)	+39.0 (−66.7)
$\mathbf{A1}_S$-$(CO)_2$	−109.2 (−220.9)	+40.8 (−80.0)	−4.3 (−117.2)	+28.5 (−81.2)
$\mathbf{A2}_S$	−359.6 (−550.1)	−212.4 (−441.4)	−271.4 (−457.2)	–
$\mathbf{A2}_S$-TS	−251.2(−424.7)	−149.6 (−368.9)	−153.0 (−337.1)	–
$\mathbf{A3}_S$	−184.8 (−303.1)	−182.4 (−331.2)	−86.8 (−208.6)	–
$\mathbf{A4}_S$	−182.2 (−351.3)	−5.8 (−214.6)	−70.6 (−232.6)	–
$\mathbf{A5}_S$	−251.2 (−434.0)	−74.4 (−302.9)	−170.2 (−358.7)	–
$\mathbf{A6}_S$	−497.0 (−615.3)	−518.6 (650.6)	−393.6 (−514.0)	–
$\mathbf{A7}_S$	−593.3 (−771.9)	−548.9 (−761.1)	−443.1 (−627.4)	–
$\mathbf{A8}_S$	−633.1 (−756.3)	−677.7 (−817.4)	−469.2 (−598.1)	–
$\mathbf{A9}_S$	−850.2 (−1031.8)	−863.4 (1083.9)	−644.5 (−828.8)	–
$\mathbf{A9}_T$	−861.7 (−1035.0)	−845.8 (−1059.8)	−657.0 (−841.1)	–

of theory predicts the reactant ground state to be diamagnetic with one amide having the expected 90° rotation, whereas the other two are rotated from axial by 18° counter to each other (see Figure 12) and make an angle of 128° with the central Ta metal. This unusual arrangement, due to the preferred metal d- and nitrogen p-orbital overlap[17] and the free ligand rotation allowed within the Model-opt level of theory, is not possible if ligand bulk is included in the optimisation. At the QM:QM level of theory the inability of the singlet to obtain its preferred geometry results in it being destabilised 21.4 kJ mol^{-1} above the triplet reactant. This allows the CO coordination to occur directly on the triplet surface forming $\mathbf{A1}_T$-CO and making $\mathbf{A1}_S$-CO an unlikely reaction coordinate.

At the Model-opt level of theory the geometries of $\mathbf{A1}_S$-$(CO)_2$ and $\mathbf{A1}_T$-$(CO)_2$ have been reversed when compared with the silox system. Although not exact replicas, the singlet now has the trigonal bipyramidal structure, whereas in the silox system it was the triplet. Our earlier examination of this bonding is displayed Figure 4, but now the HOMO and LUMO are reversed. This unusual reversal is again a result of the amide rotation, which stabilises and destabilises the previously outlined LUMO and HOMO, respectively. The HOMO, which is now the interaction between the $d_{x^2-y^2}$ and the two π* CO orbitals, forces the trigonal arrangement in the singlet.

When steric bulk is incorporated in the QM:QM analysis, the geometries are distorted once again (see Figure 13). The steric presence both inhibits amide rotation and restricts the position of the two bound CO groups in the singlet structure. In effect there is insufficient room within $\mathbf{A1}_S$-$(CO)_2$ for it to maintain its preferred orientation. This is particularly evident from the reduced angle between the bound CO groups (from 88.1° to 61.4°, see Figure 13) when steric bulk is included in the calculations. This crowding of course destabilises $\mathbf{A1}_S$-$(CO)_2$ considerably with Table 2 suggesting it is now +40.8 kJ mol^{-1} above the reactants. This destabilisation may prevent reaction through this singlet pathway.

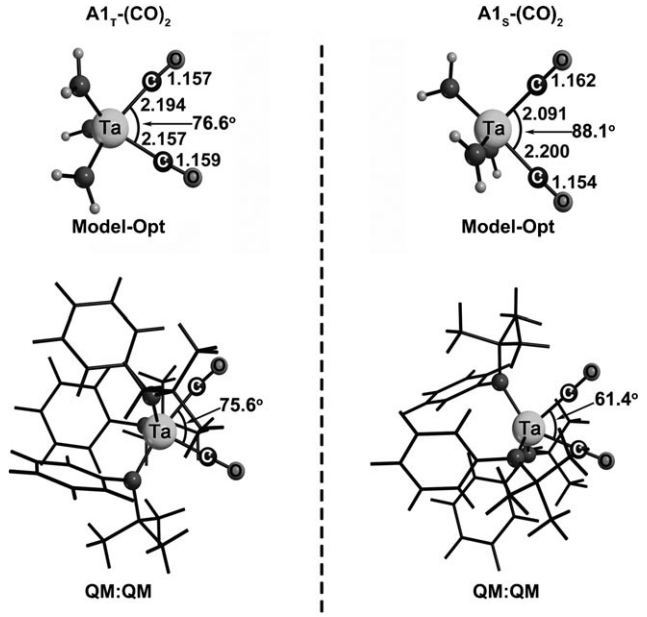

Figure 13. Model-opt and QM:QM diagrams of $\mathbf{A1}_S$-$(CO)_2$ and $\mathbf{A1}_S$-$(CO)_2$ with relevant angles highlighted.

From Figure 13, note also the arrangement of the triplet $\mathbf{A1}_T$-$(CO)_2$ at both the smaller Model-opt and bulky QM:QM levels of theory. The overall arrangement has been maintained along with the angle between the two bound CO groups. Table 2 similarly indicates less destabilisation in this structure (−20 kJ mol^{-1} below reactants), which suggests that a triplet pathway may be the preferred option.

With the path to $\mathbf{A2}_S$ via $\mathbf{A1}_S$-$(CO)_2$ being less likely, perhaps a path through this more stable triplet analogue $\mathbf{A1}_T$-$(CO)_2$ is possible. To this end, consider an alternate pathway to intermediate $\mathbf{A2}_S$ through spin pairing during coordination of a triplet reactant $\mathbf{A1}_T$ to a triplet encounter complex $\mathbf{A1}_T$-$(CO)_2$ rather than through the destabilised singlet surface. This pairing of two triplets to form a singlet is beyond our computational means at the QM:QM level of theory and unfortunately, the absence of steric effects at the Model-opt level make the calculation less meaningful. But to provide some indication that this mode of coordination is possible, we completed the Model-opt spin pairing analysis and have displayed it in Figure 14.

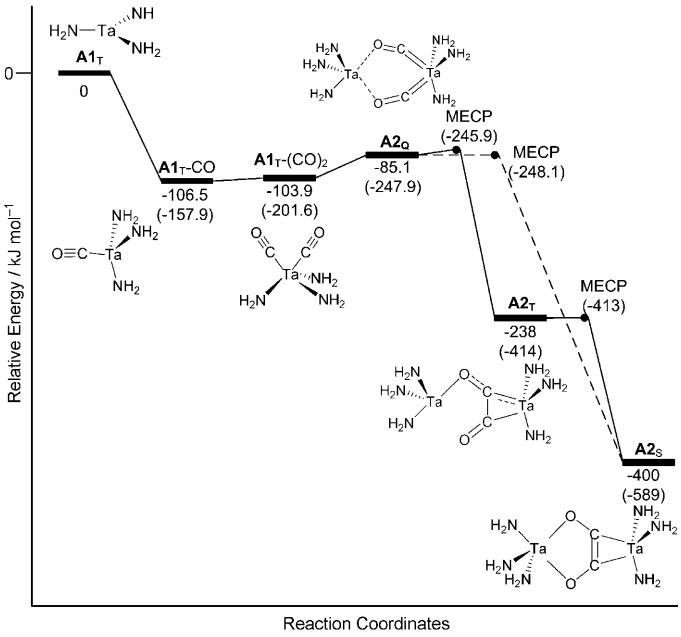

Figure 14. The $[Ta(NH_2)_3]$+CO interaction, assuming a triplet reactant ground state, at the Model-opt level of theory. Figure constructed relative to Gibbs free energies (in normal type). Values in parentheses are uncorrected electronic energies. All values in kJ mol^{-1}.

The reader should be aware that this is a guide only, but the overall profile certainly indicates a triplet $\mathbf{A1}_T$-$(CO)_2$ can coordinate with a triplet $\mathbf{A1}_T$ to form a loosely bound dinuclear Ta–$(CO)_2$–Ta quintet intermediate $\mathbf{A2}_Q$ that can immediately spin pair to the singlet. The pathway from

quintet to singlet via triplet is similarly without barrier. Given the two possible pathways available, intermediate $\mathbf{A2}_S$ will form and continue to the ketenylidene and dicarbide structures similarly found with the silox system.

Another observation made above was the slightly splayed arrangement of the central ethene 1,2-dione in $\mathbf{A2}_S$. It comes as no surprise that again the molecular orbital energies of $Ta(NH_2)_3$ are being altered by the amide rotation. The overall effect is to weaken the C–C bond and strengthen the C–O bonds, but before launching into the molecular orbital rationale, it should be remembered that the amide rotation may not be allowed if steric bulk is included. This proves to be the case as shown in Figure 15 in which the

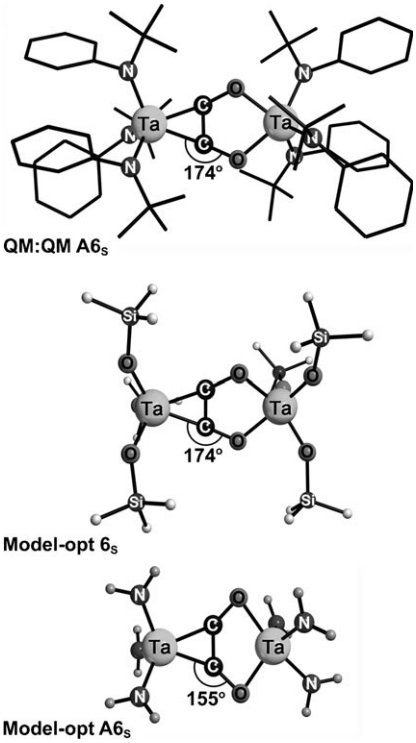

Figure 15. Moldraw diagrams of $\mathbf{A6}_S$ at both QM:QM and Model-opt level of theory and $\mathbf{6}_S$ at Model-opt level of theory.

bulky Ph and *t*Bu groups prevent amide rotation and return the splayed arrangement to that found in the silox analogue, thus maintaining the molecular orbital picture displayed in Figure 5. This effect of steric bulk countering the stabilisation due to amide rotation occurs throughout many of the structures and accounts for much of the differences between the QM:QM and Model-opt structural energetics found in Table 2.

The final observation to be considered here is in regard to the dicarbide $[(NH_2)_3Ta{-}CC{-}Ta(NH_2)_3]$ end product of this amide reaction sequence. We noted earlier that the triplet and singlet species have almost identical energies and are separated by only 4 kJ mol^{-1} at the uncorrected Model-opt level of theory, an observation also found in the silox system (see above). An analysis of the geometric arrangement of the two species finds both to have one amide rotated at each end and all bond lengths and angles comparable. The difference however, can be seen from the axial views illustrated in Figure 16. The singlet has a staggered conformation with the rotated amides on opposite sides of the molecule, whereas the triplet has a dihedral angle of around 90° between the two rotated amides.

These geometric differences were not observed with the silox system and are a consequence of the preferred metal d_{xy} and $d_{x^2-y^2}$ orbital interactions in the presence of one rotated amide group on each metal centre.[8,10,17] When steric bulk is included in the QM:QM calculations, the singlet becomes more stable than the triplet by a not insignificant (uncorrected) 24 kJ mol^{-1}. The reason for the difference is due to the singlet retaining its amide rotation (albeit with both on the same side of the molecule[54]), whereas the triplet has not. The triplet has destabilised sufficiently to allow a singlet ground state. This is opposite to that found with the original Cummins[1] dinitrogen $[Mo\{N(t\text{Bu})Ar\}_3]{-}N_2{-}[Mo\{N(t\text{Bu})Ar\}_3]$ intermediate analysed previously.[4,19] Steric bulk in that case destabilised the singlet, since it could not retain the preferred amide rotation. So why would one structure retain its amide rotation and the other not? The answer is simply geometric, with the original molybdenum structure having a shorter overall metal–metal distance that is not quite sufficient to allow free rotation.

Although the singlet ground state of an amide dicarbide can be rationalised in terms of ligand sterics, the same has not been observed for the analogous silox dicarbide. Our calculations place the silox triplet dicarbide to be lower in energy and unfortunately these molecules are (currently) computationally too large for accurate resolution of the energetic and structural intricacies. The experimental silox dicarbide crystal structure points to a distortion in the linear Ta–CC–Ta core and a slight deflection of the axial silox dihedrals, both of which are observed in our calculations with a singlet amide dicarbide, but to extrapolate these congruencies is stretching reality.

Conclusion

Experimentally, the reaction of a 3-coordinate tantalum silox species ($[Ta(silox)_3]$, silox = $OSi(t\text{Bu})_3$) and a molecule with chemistry's strongest bond, carbon monoxide, results in the formation of a dinuclear dicarbide structure of the form $[(silox)_3Ta{=}C{=}C{=}Ta(silox)_3]$. Clearly CO cleavage is required at some point in the reaction and previous theoretical analysis on the analogous Cummins style 3-coordinate tantalum amide finds that this CO cleavage can not occur via the expected Ta–CO–Ta intermediate. This intermediate structure is too stable and no further reaction from it is likely.

In this theoretical study we have shown that if an intermediate of the general formula $Ta{-}C_nO{-}Ta$ is formed, in which n is an even number, the intermediate is less stable and, hence further reaction (or specifically CO cleavage) is

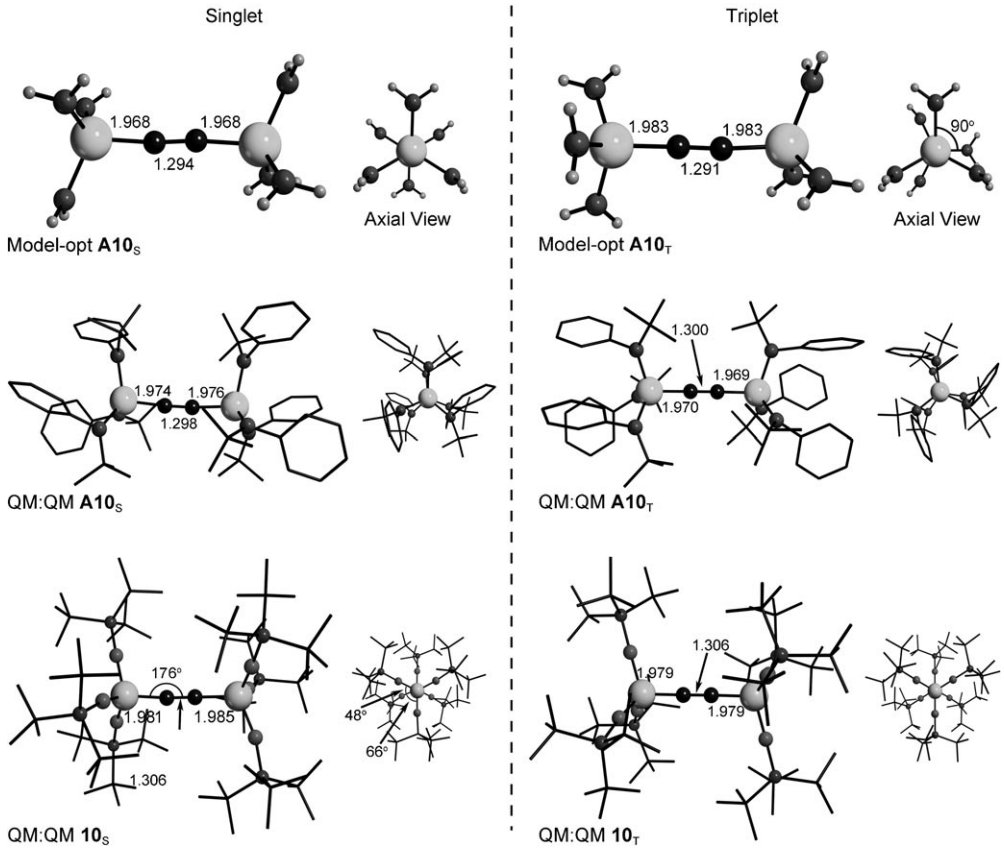

Figure 16. Moldraw diagrams of singlet and triplet dicarbide for both the silox and amide systems. Hydrogen atoms are omitted from the QM:QM diagrams. All values in Å.

possible. This is exactly the case with the experimental tantalum silox and CO reaction. A precursor to this intermediate, $[(silox)_3Ta{-}CCO]$, has been observed and characterised from which further reaction (CO cleavage) gives a dicarbide. Our analysis has found that once formed the Ta–CCO–Ta intermediate cleaves the C–O bond to form Ta=C=C: and Ta=O, and should additional reactant be present provides the Ta=C=C=Ta dicarbide end product.

This finding is individually interesting, but the mechanistic pathway to form the intermediate $Ta{-}C_nO{-}Ta$ (or its precursor $Ta{-}C_nO$) has also been identified. Starting from the reactant we find that two CO molecules can bind with one tantalum silox reactant forming an unstable intermediate of the form $[(silox)_3Ta{-}(CO)_2]$. The two CO groups, bound through the carbon, are in a *cis* arrangement whereby an additional $[Ta(silox)_3]$ reactant can coordinate to the oxygen atoms creating a more stable intermediate of the form $[(silox)_3Ta{-}(CO)_2{-}Ta(silox)_3]$. It is this intermediate structure that has eluded experimental characterisation. It consists of a non-linear ethene 1,2-dione (O-C-C-O) wedged between the two metal centres such that the central carbon–carbon bond has been stabilised by electron donation from the metal atoms. This electron donation into the symmetry-adapted π bonding/antibonding orbitals has the simultaneous effect of activating the carbon oxygen bonds such that cleavage over a modest transition barrier is possible. Once one CO cleavage occurs, a stable (isolatable) ketenylidene of the form $[(silox)_3Ta{-}CCO]$ is created that has the necessary $Ta{-}C_nO$ (in which n is even) arrangement from which further cleavage can occur.

Our analysis has highlighted other potential, although less likely, pathways to the ketenylidene. One involves first forming the stable Ta–CO–Ta intermediate followed by attack on the central CO by a second carbon monoxide molecule. Although thermodynamically less likely, we have found a major barrier to this reaction comes from the steric protection afforded to the centrally bound CO molecule by the encompassing cage structure of the silox ligands. Removal of this barrier can occur by a variation to this path, which involves interaction in a head-to-head fashion of two $[(silox)_3Ta{-}CO]$ structures. The head-to-head reaction actually results in dissociation of one CO group, but now it is caught within the steric cage provided by the silox ligands. This second pathway is certainly possible, but thermodynamics would suggest it to be less likely.

In the course of our analysis we have highlighted the potential for altering the reacting metal to form a mixed-metal intermediate of the form $[(silox)_3Ta{-}(CO)_2{-}M(silox)_3]$. Preliminary analysis would suggest this is possible for electron-rich metals to the right of tantalum in the periodic table, such as tungsten and rhenium, but not for electron-deficient metals to the left of tantalum, such as hafnium or lantha-

num. We have also provided a detailed analysis in which the ligand arrangement of the silox groups has been changed to the Cummins-style three-coordinate amide system. Our findings in this regard are that the three-coordinate amide reaction should progress in almost identical fashion to a tantalum amide dicarbide via the ketenylidene intermediate. In fact, the amide system shows greater stability of all species relative to the reactants when compared with the silox system, which is due to the (well-studied) amide rotation, which provides greater electron density to the central axis of the species.

We conclude here by highlighting the importance of the yet to be experimentally characterised (red) intermediate $[(silox)_3Ta{-}(CO)_2{-}Ta(silox)_3]$. We have shown it to be a non-linear ethene 1,2-dione (O-C-C-O) wedged between the two metal centres. The carbon–carbon bond is well formed making this observed, but unstable intermediate a natural precursor for further reactions. The structure may require judicious tuning of the ligand system to alter the steric cage surrounding the intermediate, but as we have shown this could be achieved by switching to the Cummins amide system.

[1] C. E. Laplaza, C. C. Cummins, *Science* **1995**, *268*, 861.
[2] R. R. Schrock, *Chem. Commun.* **2003**, 2389.
[3] N. J. Brookes, A. Ariafard, R. Stranger, B. F. Yates, *Dalton Trans.* **2009**, 9266.
[4] N. J. Brookes, D. C. Graham, G. J. Christian, R. Stranger, B. F. Yates, *J. Comput. Chem.* **2009**, *30*, 2146.
[5] Q. Cui, D. G. Musaev, M. Svensson, S. Sieber, K. Morokuma, *J. Am. Chem. Soc.* **1995**, *117*, 12366.
[6] A. R. Johnson, W. M. Davis, C. C. Cummins, S. Serron, S. P. Nolan, D. G. Musaev, K. Morokuma, *J. Am. Chem. Soc.* **1998**, *120*, 2071.
[7] D. V. Khoroshun, D. G. Musaev, K. Morokuma, *Organometallics* **1999**, *18*, 5653.
[8] G. Christian, J. Driver, R. Stranger, *Faraday Discuss.* **2003**, *124*, 331.
[9] G. Christian, R. Stranger, *Dalton Trans.* **2004**, 2492.
[10] G. Christian, R. Stranger, D. C. Graham, B. F. Yates, *Dalton Trans.* **2005**, *5*, 962.
[11] G. Christian, R. Stranger, S. Petrie, B. F. Yates, C. C. Cummins, *Chem. Eur. J.* **2007**, *13*, 4264.
[12] G. Christian, R. Stranger, B. F. Yates, C. C. Cummins, *Eur. J. Inorg. Chem.* **2007**, 3736.
[13] G. Christian, R. Stranger, B. F. Yates, C. C. Cummins, *Dalton Trans.* **2007**, 1939.
[14] G. Christian, R. Stranger, B. F. Yates, C. C. Cummins, *Dalton Trans.* **2008**, 338.
[15] G. J. Christian, R. Stranger, B. F. Yates, *Inorg. Chem.* **2006**, *45*, 6851.
[16] A. Ariafard, N. J. Brookes, R. Stranger, B. F. Yates, *J. Am. Chem. Soc.* **2008**, *130*, 11928.
[17] A. Ariafard, N. J. Brookes, R. Stranger, B. F. Yates, *Chem. Eur. J.* **2008**, *14*, 6119.
[18] D. C. Graham, G. J. O. Beran, M. Head-Gordon, G. Christian, R. Stranger, B. F. Yates, *J. Phys. Chem. A* **2005**, *109*, 6762.
[19] J. J. Curley, T. R. Cook, S. Y. Reece, P. Müller, C. C. Cummins, *J. Am. Chem. Soc.* **2008**, *130*, 9394.
[20] B. Le Guennic, B. Kirchner, M. Reiher, *Chem. Eur. J.* **2005**, *11*, 7448.
[21] R. Stranger, B. F. Yates, *Chem. Phys.* **2006**, *324*, 202.
[22] J. Hahn, C. R. Landis, V. A. Nasluzov, K. M. Neyman, N. Rosch, *Inorg. Chem.* **1997**, *36*, 3947.
[23] K. M. Neyman, V. A. Nasluzov, J. Hahn, C. R. Landis, N. Rosch, *Organometallics* **1997**, *16*, 995.
[24] D. R. Neithamer, R. E. LaPointe, R. A. Wheeler, D. S. Richeson, G. D. Van Duyne, P. T. Wolczanski, *J. Am. Chem. Soc.* **1989**, *111*, 9056.
[25] R. E. LaPointe, P. T. Wolczanski, J. F. Mitchell, *J. Am. Chem. Soc.* **1986**, *108*, 6382.
[26] Molecule identification is by a structure number in bold, followed by a subscript indicating its spin state (S = singlet, T = triplet) and the attached group symbol (should one be present). Transition structures are signified by a TS. All structures applied to the Laplaza–Cummins tri-amide system $[M\{N(t\mathrm{Bu})Ar\}_3]$ are prefixed with an A in bold.
[27] D. S. Kuiper, P. T. Wolczanski, E. B. Lobkovsky, T. R. Cundari, *J. Am. Chem. Soc.* **2008**, *130*, 12931.
[28] A. D. Becke, *Phys. Rev. A* **1988**, *38*, 3098.
[29] A. D. Becke, *J. Chem. Phys.* **1993**, *98*, 5648.
[30] C. Lee, W. Yang, R. G. Parr, *Phys. Rev. B* **1988**, *37*, 785.
[31] P. J. Stephens, F. J. Devlin, C. F. Chabalowski, M. J. Frisch, *J. Phys. Chem.* **1994**, *98*, 11623.
[32] P. J. Hay, W. R. Wadt, *J. Chem. Phys.* **1985**, *82*, 299.
[33] W. R. Wadt, P. J. Hay, *J. Chem. Phys.* **1985**, *82*, 284.
[34] W. J. Hehre, L. Radom, P. R. Schleyer, J. A. Pople, *AB INITIO Molecular Orbital Theory*, 1st ed., Wiley-Interscience, New York, **1986**.
[35] J. P. Perdew, *Phys. Rev. B* **1986**, *33*, 8822.
[36] A. D. McLean, G. S. Chandler, *J. Chem. Phys.* **1980**, *72*, 5639.
[37] S. Dapprich, I. Komaromi, K. S. Byun, K. Morokuma, M. J. Frisch, *J. Mol. Struct.* **1999**, *474–515*, 1.
[38] K. Morokuma, *Bull. Korean Chem. Soc.* **2003**, *24*, 797.
[39] K. Morokuma, D. G. Musaev, D. V. Khoroshun, T. Vreven, Z. W. Liu, M. Torrent, H. Basch, B. F. Yates, S. Mori, *Abstr. Pap. Am. Chem. Soc.* **2000**, *220*, U492.
[40] Gaussian 03, Revision E.01, M. J. Frisch, G. W. Trucks, H. B. Schlegel, G. E. Scuseria, M. A. Robb, J. R. Cheeseman, J. A. Montgomery, Jr., T. Vreven, K. N. Kudin, J. C. Burant, J. M. Millam, S. S. Iyengar, J. Tomasi, V. Barone, B. Mennucci, M. Cossi, G. Scalmani, N. Rega, G. A. Petersson, H. Nakatsuji, M. Hada, M. Ehara, K. Toyota, R. Fukuda, J. Hasegawa, M. Ishida, T. Nakajima, Y. Honda, O. Kitao, H. Nakai, M. Klene, X. Li, J. E. Knox, H. P. Hratchian, J. B. Cross, V. Bakken, C. Adamo, J. Jaramillo, R. Gomperts, R. E. Stratmann, O. Yazyev, A. J. Austin, R. Cammi, C. Pomelli, J. W. Ochterski, P. Y. Ayala, K. Morokuma, G. A. Voth, P. Salvador, J. J. Dannenberg, V. G. Zakrzewski, S. Dapprich, A. D. Daniels, M. C. Strain, O. Farkas, D. K. Malick, A. D. Rabuck, K. Raghavachari, J. B. Foresman, J. V. Ortiz, Q. Cui, A. G. Baboul, S. Clifford, J. Cioslowski, B. B. Stefanov, G. Liu, A. Liashenko, P. Piskorz, I. Komaromi, R. L. Martin, D. J. Fox, T. Keith, M. A. Al-Laham, C. Y. Peng, A. Nanayakkara, M. Challacombe, P. M. W. Gill, B. Johnson, W. Chen, M. W. Wong, C. Gonzalez, J. A. Pople, Gaussian, Inc., Wallingford CT, **2004**.
[41] A. K. Rappe, C. J. Casewit, K. S. Colwell, W. A. Goddard, W. M. Skiff, *J. Am. Chem. Soc.* **1992**, *114*, 10024.
[42] C. Gonzalez, H. B. Schlegel, *J. Phys. Chem.* **1990**, *94*, 5523.
[43] J. N. Harvey, M. Aschi, *Phys. Chem. Chem. Phys.* **1999**, *1*, 5555.
[44] J. N. Harvey, M. Aschi, H. Schwarz, W. Koch, *Theor. Chem. Acc.* **1998**, *99*, 95.
[45] T. Ziegler, *Chem. Rev.* **1991**, *91*, 651.
[46] N. Koga, K. Morokuma, *Chem. Rev.* **1991**, *91*, 823.
[47] G. Frenking, N. Frohlich, *Chem. Rev.* **2000**, *100*, 717.
[48] Although beyond the scope of this manuscript, the THF adduct analysis also reveals interesting subtleties. One being the two silox environments noted experimentally in THF-$\mathbf{1}_S$-CO adduct at −110 °C that coalesce on warming. Our calculations indicate that the only case in which two silox environments exist is for the singlet THF-$\mathbf{1}_S$-CO adduct, hence the warming may be providing the experimentalists with an observable spin crossing.
[49] To substantiate this claim we tested this structure by replacing the Ta metal with Re, which has two additional electrons. The lowest energy conformer obtained has a distorted square pyramidal structure, but a higher energy conformer exists in which the C=C has

formed. This C=C bond does not exist with the Ta structure (see the Supporting Information).

[50] E. L. Werkema, L. Maron, O. Eisenstein, R. A. Andersen, *J. Am. Chem. Soc.* **2007**, *129*, 2529.

[51] Note that electron donation from both metals is required to form the $\mathbf{2_S}$ structure. For example, the structure Re–$(CO)_2$–La will not form despite being isoelectronic with Ta–$(CO)_2$–Ta.

[52] For purely speculative curiosity we again considered the case of altering one metal centre to create electron rich/deficient situations. The LUMO in this case creating a slightly different structure for the tungsten and rhenium analogues (see the Supporting Information).

[53] C. E. Laplaza, M. J. A. Johnson, J. C. Peters, A. L. Odom, E. Kim, C. C. Cummins, G. N. George, I. J. Pickering, *J. Am. Chem. Soc.* **1996**, *118*, 8623.

[54] Conformer searching at the Model-opt level of theory located two low energy structures, separated by less than 1 $kJ\,mol^{-1}$. The lowest energy conformer had the two rotated amides on opposite sides of the molecule and the slightly higher energy conformer had them on the same side of the molecule. Inclusion of steric bulk at the QM:QM level of theory has favoured the latter conformer over the former.

Received: December 7, 2009
Published online: June 10, 2010

